

Dielectric properties and phase transitions of [001], [110], and [111] oriented $\text{Pb}(\text{Zn}_{1/3}\text{Nb}_{2/3})\text{O}_3$ -6% PbTiO_3 single crystals

Mouhamed Amin Hentati,^{1,2} Hichem Dammak,¹ Hamadi Khemakhem,² and Mai Pham Thi³

¹Laboratoire Structures, Propriétés et Modélisation des Solides UMR 8580 CNRS, Ecole Centrale de Paris, 92295 Châtenay-Malabry, France

²Laboratoire des Matériaux Ferroélectriques—Faculté des Sciences de Sfax—Route Soukra Km 3,5, B.P.802,3018 Sfax, Tunisia

³Laboratoire Nanocomposites & Matériaux Hétérogènes, THALES Research & Technology-France, RD 128, F-91767 Palaiseau cedex, France

(Received 7 April 2013; accepted 10 June 2013; published online 27 June 2013)

Phase transformations of [001], [110], and [111] oriented $\text{Pb}(\text{Zn}_{1/3}\text{Nb}_{2/3})\text{O}_3$ -6% PbTiO_3 (PZN-6%PT) single crystals have been investigated by means of dielectric permittivity and loss, x-ray diffraction and depolarization current as function of temperature (from 250 to 500 K). The unpoled samples undergo R-T-C phase transition sequence during zero field heating (ZFH), where R, T, and C are rhombohedral, tetragonal, and cubic phases, respectively. Under electric field (0.5 kV/cm), an intermediate orthorhombic (O) phase is induced between the T and R phases in the field cooling (FC) process. This phase reappears during subsequent zero field heating of the poled sample (zero field heating after field cooling: ZFHaFC). The existence range of this O phase depends on both the crystal orientation and the measurement conditions (FC or ZFHaFC). Finally, for the [001] direction, it was found that the piezoelectric activity of the intermediate phase is the highest.

© 2013 AIP Publishing LLC. [<http://dx.doi.org/10.1063/1.4812327>]

I. INTRODUCTION

Solid solution of the complex perovskite $\text{Pb}(\text{Zn}_{1/3}\text{Nb}_{2/3})\text{O}_3$ (PZN) and the simple ferroelectric PbTiO_3 (PT) have attracted a huge amount of attention over the last decades. Indeed, $(1-x)\text{Pb}(\text{Zn}_{1/3}\text{Nb}_{2/3})\text{O}_3$ - $x\text{PbTiO}_3$ (PZN- $x\%$ PT) single crystals, with $0\% \leq x \leq 10\%$, exhibit ultrahigh piezoelectric coefficient ($d_{33} \geq 1100\text{pC/N}$), extremely large piezoelectric strain levels ($>1\%$) and a very high electromechanical coupling factor ($k_{33} \geq 85\%$).¹ Such properties made them very attractive for practical applications, as actuators and sensors used in ultrasonic transducers.²⁻⁴ From materials science point of view, these interesting electromechanical properties are generally attributed to a strong “polarization rotation effect” under electric field.⁵ Nowadays, it is well known that the magnitude of piezoelectric coefficients depends on the direction of the spontaneous polarization (the microscopic symmetry) and the orientation of the poling electric field.¹ However, the microscopic symmetry and thus the ferroelectric transition sequence of PZN- $x\%$ PT single crystals strongly depend not only on the poling orientation but also the thermo-electrical process applied: zero field cooling (ZFC), zero field heating (ZFH), field cooling (FC), field heating (FH), zero field heating after field cooling (ZFHaFC), zero field cooling after field heating (ZFCaFH), and increasing field (IF) process.⁶⁻⁸

In this paper, we report the results of the dielectric and the x-ray diffraction (XRD) study of [001], [110], and [111] oriented PZN-6%PT single crystals under different thermo-electrical processes. Depolarization current was performed in order to study the domain structure stability.

II. EXPERIMENTAL PROCEDURE

$\text{Pb}(\text{Zn}_{1/3}\text{Nb}_{2/3})\text{O}_3$ -6% PbTiO_3 (PZN-6%PT) single crystals were grown using the conventional high temperature flux method described elsewhere.^{9,10} Crystals were oriented, by the Laue backscattering method, along [001], [110], and [111] pseudocubic directions and cut with wire-saw. Samples were then polished and gold electrodes were sputtered on their relevant faces. Dielectric measurements were performed, at 10 kHz, using HP4192 LF impedance analyzer connected with a computer controlled temperature chamber. These measurements were made over a temperature range of 250–500 K on heating and cooling, with a rate of 2 K/min. In the experiments, the dielectric properties of the samples were measured using four different process: (i) ZFC process, in which the unpoled sample was cooled down from 500 K under zero dc bias to 250 K; (ii) ZFH process, in which the sample was heated under zero dc bias from 250 to 500 K; (iii) FC process, in which the unpoled sample was cooled down from 500 K under a constant dc bias to 250 K; and (iv) ZFHaFC process, in which the FC-poled sample was heated under zero dc bias from 250 to 500 K. The pyroelectric current has been measured using a Keithley 617 electrometer in ZFHaFC process.

The XRD patterns were recorded with a high-resolution two-axes diffractometer, using $\text{Cu } K_\beta$ ($\lambda = 0.139223 \text{ nm}$) monochromatic radiation issued from a Rigaku rotating anode (RU300, 18 kW). The powder sample was obtained by grinding single crystals at room temperature. The powder was sieved ($d \leq 50 \mu\text{m}$) and then annealed at 470 K in order to reduce strains induced by grinding. Samples (single crystal or powder) were fixed on a copper holder inside a N_2 flow

cryostat (80–470 K) mounted on a HUBER goniometric head. In the Bragg–Brentano geometry, the diffraction angles were measured with a relative precision better than 0.002° (2θ).

To optimize the poling electric field necessary to obtain an “optimally poled sample,” we measured macroscopic polarization developed by 0.25, 0.5, and 1 kV/cm fields cooling from 500 K to room temperature. Fig. 1 shows that a field of 0.5 kV/cm is enough to pole the samples in the [001] direction. Thus, [001] oriented crystals were poled in FC (0.5 kV/cm) process, and electromechanical properties were determined as function of temperature by the resonance-antiresonance method according to IEEE norm¹¹ using HP 4192 impedance analyzer.

III. RESULTS AND DISCUSSIONS

A. Phase transitions in PZN-6%PT at zero E field

The thermal evolution of dielectric permittivity and loss of an unpoled [111] single crystal platelet, for ZFH scheme, is given in Fig. 2(a). The real part of dielectric permittivity shows three anomalies around 388 K, 426 K (the “shoulder” in the permittivity), and 432 K (for 10 kHz). The last temperature is the temperature of maximum permittivity, $T_m(f)$, which strongly depends on frequency and is characteristics of relaxor state. It does not correspond to a classical phase transition. The two other temperatures (marked with peaks in dielectric loss) can be associated to structural phase transitions. The superposition of the dielectric permittivity in ZFC and ZFH processes shows the presence of two thermal hysteresis (in the vicinity of the phase transition temperatures) indicating both are first order phase transitions.¹²

The evolution of the (002), (220), and (222) pseudocubic reflections as a function of temperature suggests that, like unpoled PZN-4.5%PT,^{6,13–15} unpoled PZN-6%PT single crystal undergoes, upon heating, a R-T-C phase transition sequence, where R, T, and C are rhombohedral, tetragonal, and cubic phases, respectively. These transformations occur over a temperature range marked by the coexistence of the low and the high temperature phases, confirming that such transitions are first order. This is in good agreement with the

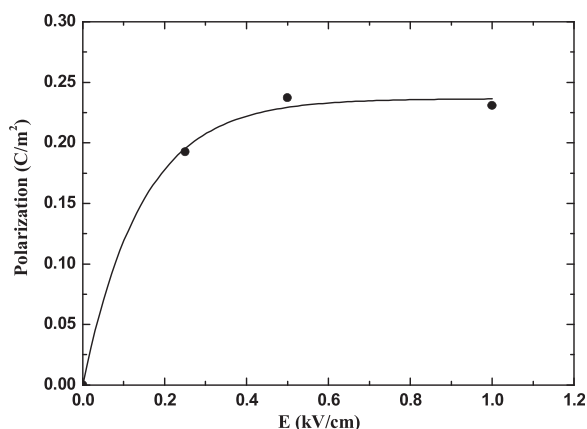


FIG. 1. Spontaneous polarizations at room temperature for [001] oriented PZN-6%PT single crystal poled with different electric fields during FC process from 500 K to room temperature.

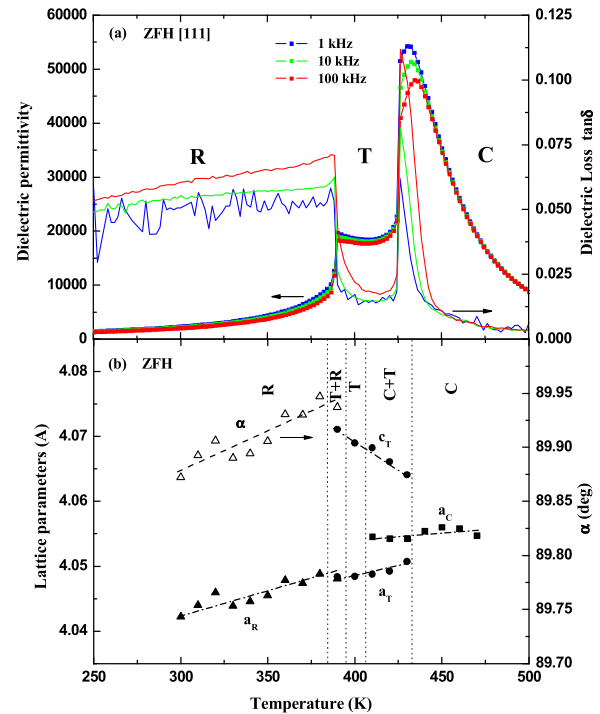


FIG. 2. Temperature dependence of (a) the dielectric permittivity and loss of unpoled [111] oriented PZN-6%PT single crystal and (b) the lattice parameters of PZN-6%PT powder.

results previously reported in annealed PZN-4.5%PT¹⁵ and PZN-6%PT.¹⁶ Fig. 2(b) shows the evolution of the extracted cell parameters of these phases during the ZFH process.

B. Phase transitions in FC condition

1. [110] Oriented single crystal

Fig. 3(a) shows the temperature dependence of the dielectric permittivity ($\epsilon_{33}^T/\epsilon_0$) and the dielectric loss ($\tan\delta$) carried out on a [110]-oriented single crystal, in FC (0.5 kV/cm) condition. X-ray investigations were performed on the same single crystal during the FC process and the temperature dependence of the inter-planar spacing d_{330} is given in Fig. 3(b).

Both $\epsilon_{33}^T/\epsilon_0$ and d_{330} measurements show three abrupt variations during the FC (0.5 kV/cm) process, characteristic of phase transitions, at $T \approx 425$, 370, and 325 K. So, an intermediate phase is induced between the T and R ones. In the temperature range of this phase (325–370 K), the permittivity $\epsilon_{33}^T/\epsilon_0$ is lowest and the reticular distance d_{330} is the highest than for other temperatures. This behavior indicates that the polar axis of the intermediate phase is close to [110] and the phase symmetry should be orthorhombic (O). This induced O phase is typical of field cooled [110] oriented PZN-PT and PMN-PT: $((1-x)\text{PbMg}_{1/3}\text{Nb}_{2/3}\text{O}_3-x\text{PbTiO}_3)$ single crystals near the morphotropic phase boundary.^{6–8,17–21}

For the low temperature symmetry, recent study of [110] field cooled PZN-4.5%PT, using high precision x-ray diffraction, suggests that the application of electric field transform the R phase to a monoclinic M_B one.⁸ However, Wang demonstrated that the nanotwin superlattices of rhombohedral phase diffract x-ray incident waves just like monoclinic M_B phase.²² Therefore, this apparent monoclinic phase

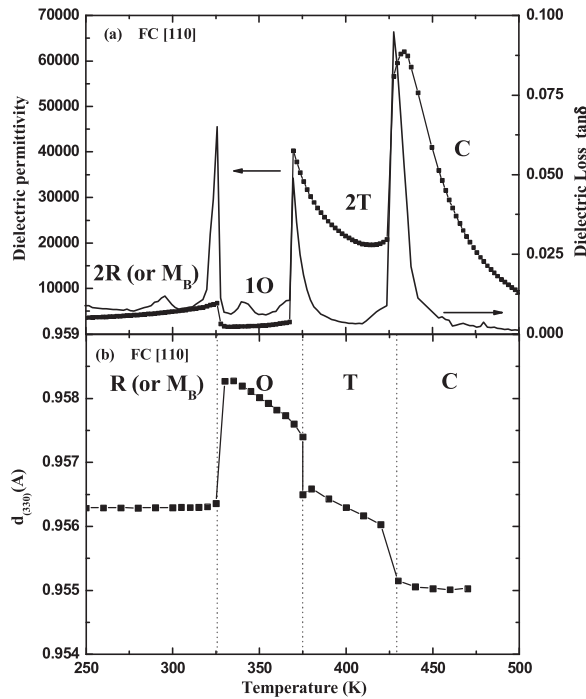


FIG. 3. Temperature dependence of (a) the dielectric permittivity and loss at 10kHz and (b) the inter-planer spacing d_{330} of [110] oriented PZN-6%PT single crystal during FC process.

could be caused by the presence of stressed rhombohedral nanodomains.

Therefore, under FC process, [110] oriented PZN-6%PT single crystal undergoes C-T-O-R (or M_B) phase transition sequence, which leads to the following domain configurations: 2T–1O–2R (or $2M_B$) (the digit stands for the number of equivalent ferroelectrics domains).⁶

2. [001] Oriented single crystal

The temperature dependence of $\epsilon_{33}^T/\epsilon_0$ (Fig. 4(a)) and d_{004} (Fig. 4(b)) shows three phase transitions, at $T \approx 430$, 355, and 325 K. In the temperature range 355–430 K, the dielectric permittivity $\epsilon_{33}^T/\epsilon_0$ is the lowest and the inter-planer spacing d_{004} is the highest. This behavior is in agreement with tetragonal single domain state (1T). We suggest that the other two phases are orthorhombic (O) and rhombohedral (R) similar to those observed in [110] oriented single crystal. At the T-O and O-R phase transition temperatures, the dielectric permittivity increases according to the formation of the multidomain poled states 4O and 4R. The temperature range of the stability of the 4O state (30 K) is lower than that of the 1O state (45 K). This transformation sequence is consistent with that previously reported on PZN-4.5%PT.⁶

3. [111] Oriented single crystal

Three anomalies were detected (for $T \approx 425$, 368, and 364 K) from the dielectric data (Fig. 5(a)), which we assume to be associated to the C-T-O-R phase transition sequence. Compared to the other crystallographic directions, the temperature range of the orthorhombic phase is very narrow (~ 4 K). This is not surprising because the applied [111]

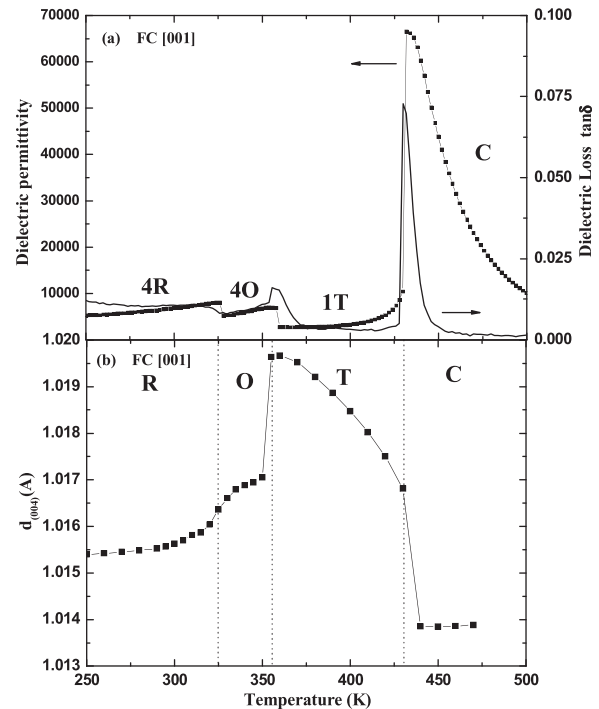


FIG. 4. Temperature dependence of (a) the dielectric permittivity and loss at 10kHz and (b) the inter-planer spacing d_{004} for [001] oriented PZN-6%PT single crystal during FC process.

electric field acted to stabilize the low temperature rhombohedral (R) phase. This explains why only two anomalies are shown by the inter-planer spacing d_{222} curve (Fig. 5(b)): the temperature range of the O phase (~ 4 K) is much smaller than the measurement step which is equal to 10 K. In the case of PZN-4.5%PT, Shen and Cao proved that the induced O phase disappears when the electric field exceeds a threshold value.²³

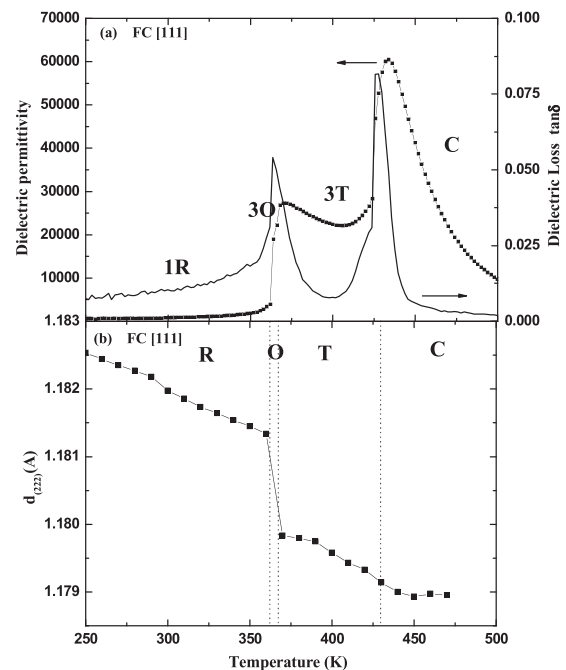


FIG. 5. Temperature dependence of (a) the dielectric permittivity and loss at 10kHz and (b) the inter-planer spacing d_{222} for [111] oriented PZN-6%PT single crystal during FC process.

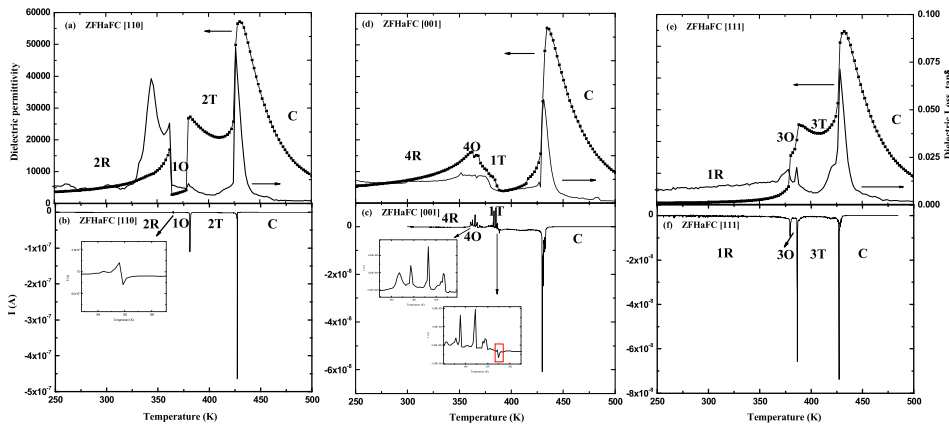


FIG. 6. Temperature dependence of the dielectric permittivity and loss at 10 kHz for PZN-6%PT single crystal during ZFHaFC process oriented along (a) [110], (c) [001], and (e) [111]. Thermal depolarization current for PZN-6%PT single crystal during ZFHaFC process oriented along (b) [110], (d) [001], and (f) [111].

Consequently, under field cooling, [111] oriented PZN-6%PT single crystal undergoes C-T-O-R phase transition sequence of the following domain configurations: 3T-3O-1R.

C. Phase transition and domain structure stability in ZFHaFC condition

Fig. 6 illustrates the zero field heating after field cooling (ZFHaFC) dielectric permittivity, dielectric loss, and thermal depolarization current data, collected for [110], [001], and [111] oriented single crystals, respectively.

For [110] oriented crystal, three anomalies are present in the dielectric permittivity (Fig. 6(a)) and in the thermal depolarization current (Fig. 6(b)), demonstrating the stability of the induced O phase in a temperature range (14 K) much smaller than for the FC process (45 K). In contrast to the dielectric permittivity characterized by a dramatic drop at the transition 2R-1O, the pyroelectric current shows a small signal indicating a tiny variation of the polarization during this transition. Thus, in a ZFHaFC process, [110] PZN-6%PT single crystal undergoes R-O-T-C phase transitions sequence.

Fig. 6(c) shows the thermal depolarization current obtained from the [001] sample. Below 360 K the current is very low showing a good stability of the polarization. In the temperature ranges 361–369 K and 382–387 K, multiple but relatively weak current signals were measured and are associated to the phase transitions from 4R to 4O, and from 4O phase to 1T states, respectively. Above a temperature of 388 K, a negative current is observed indicating a partial depolarization of the single domain state 1T. This partial depolarization is in agreement with the value of the dielectric constant (4000–10 000, Fig. 6(c)) in the temperature range 388–420 K which is higher than that measured for the 1T state during FC (3000–5000, Fig. 4(a)). Finally, a very strong current peak, corresponding to the transition from T to C phase, was detected at about 430 K. In conclusion, the ZFHaFC [001] PZN-6%PT single crystal undergoes R-O-T-C phase transition sequence.

Finally, based on the results obtained from the [110] and [001] directions, the anomalies shown in the dielectric permittivity (Fig. 6(e)) and the thermal depolarization current (Fig. 6(f)) in the [111]_C oriented sample could be associated with the R-O-T-C phase transition sequence of 1R-3O-3T domain states, respectively.

D. Temperature dependence of electromechanical properties

The piezoelectric coefficient $d_{31}^{[001]_c/[100]_c}$ and the electro-mechanical coupling factor $k_{31}^{[001]_c/[100]_c}$ of [001] oriented PZN-6%PT single crystal, poled in FC (0.5 kV/cm) process, were determined (in ZFHaFC conditions) as a function of temperature. Above 390 K, i.e., in the T phase, it was not possible to extract electromechanical properties, since the impedance spectrum shows an additional parasitic vibration mode confirming the above mentioned instability of the 1T state. For this reason, we present the temperature dependence of electromechanical properties from 250 to 380 K. In the R phase the piezoelectric coefficient $d_{31}^{[001]_c/[100]_c}$ was found to increase with increasing temperature from 810 pC/N at

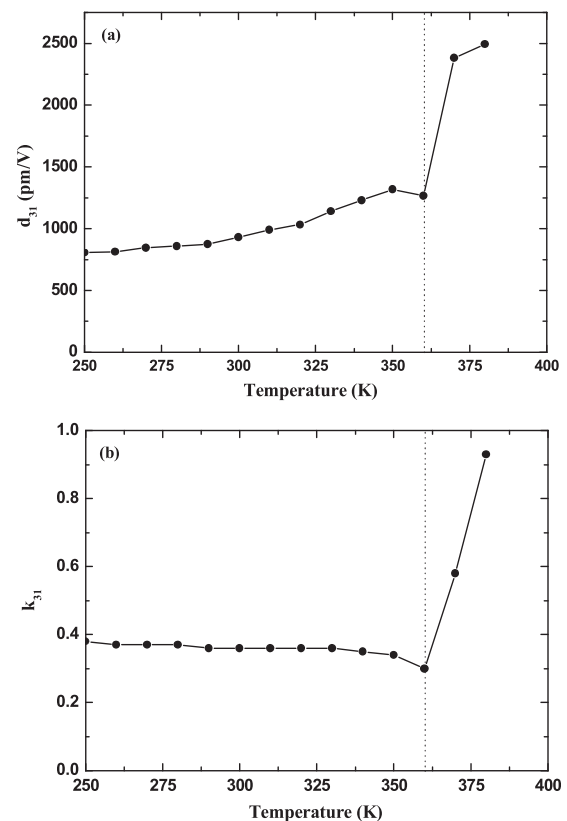


FIG. 7. Temperature dependence of the (a) piezoelectric coefficient $d_{31}^{[001]_c/[100]_c}$ and the (b) electromechanical coupling factor $k_{31}^{[001]_c/[100]_c}$ of [001] oriented PZN-6%PT single crystal.

250 K to 1320 pC/N at 350 K (Fig. 7(a)). An abrupt change of the piezoelectric coefficient occurs with the R - O phase transition and it reaches a value of 2400 pC/N in the O phase. The electromechanical coupling factor $k_{31}^{[001]_c/[100]_c}$ remains stable in the R phase (≈ 0.35) with increasing temperature (Fig. 7(b)), which is important for applications requiring thermal stability, and then increases sharply above the R-O phase transition.

IV. CONCLUSION

In summary, dielectric and XRD measurements of $[001]_c$, $[110]_c$, and $[111]_c$ oriented PZN-6%PT crystals have been performed. The unpoled samples undergo R-T-C first order phase transition sequence during ZFH. Under electric field (0.5 kV/cm), an intermediate O phase is induced between T and R phases. This phase reappears during subsequent zero field heating of the poled sample. Therefore, a C-T-O-R phase transition sequence was found in the FC and the reverse transitions in the ZFHaFC process. The domain state of this O phase depends both on the crystal orientation and the measurement conditions. For $[001]_c$ direction, in ZFHaFC process, a domain structure instability occurs in the T phase temperature range. Finally, for the $[001]$ direction, it was found that the piezoelectric activities of the intermediate phase are the highest.

ACKNOWLEDGMENTS

The authors are grateful to French government for financial support.

¹S.-E. Park and T. R. Shrout, *J. Appl. Phys.* **82**, 1804 (1997).

²A.-E. Renault, H. Dammak, P. Gaucher, M. P. Thi, and G. Calvarin, in *Proceeding of the 13th IEEE ISAF* (2002), p. 439.

³T. Ritter, X. Geng, K. Kirk Shung, P. D. Lopath, S.-E. Park, and T. R. Shrout, *IEEE Trans. Ultrason. Ferroelectr. Freq. Control* **47**, 792 (2000).

⁴S.-E. Park and T. R. Shrout, *IEEE Trans. Ultrason. Ferroelectr. Freq. Control* **44**, 1140 (1997).

⁵H. Fu and R. E. Cohen, *Nature* **403**, 281 (2000).

⁶A. E. Renault, H. Dammak, G. Calvarin, P. Gaucher, and M. P. Thi, *J. Appl. Phys.* **97**, 044105 (2005).

⁷Y. Lu, D.-Y. Jeong, Z.-Y. Cheng, T. R. Shrout, and Q. M. Zhang, *Appl. Phys. Lett.* **80**, 1918 (2002).

⁸J. Yao, H. Cao, W. Ge, J. Li, and D. Viehland, *Appl. Phys. Lett.* **95**, 052905 (2009).

⁹A.-E. Renault, H. Dammak, G. Cabvarin, M. P. Thi, and P. Gaucher, *Jpn. J. Appl. Phys., Part 1* **41**, 3846 (2002).

¹⁰S. J. Zhang, L. Lebrun, S. Rhee, R. E. Eitel, C. A. Randall, and T. R. Shrout, *J. Cryst. Growth* **236**, 210 (2002).

¹¹IEEE Ultrasonics, Ferroelectrics, and Frequency Control Society, The Institute of Electrical and Electronics Engineers, IEEE Standard on Piezoelectricity IEEE, ANSI/IEEE Standard No. 176-1987 (1987).

¹²M. E. Lines and A. M. Glass, *Principles and Applications of Ferroelectrics and Related Materials* (Clarendon Press, Oxford, 1975).

¹³J. S. Forrester, E. H. Kisi, and K. S. Knight, *Physica B* **385-386**, 160 (2006).

¹⁴J. S. Forrester, R. O. Piltz, E. H. Kisi, and G. J. McIntyre, *J. Phys.: Condens. Matter* **13**, 825 (2001).

¹⁵L. C. Lim, W. S. Chang, K. K. Rajan, M. Shanthi, P. Yang, H. O. Moser, C.-S. Tu, F.-T. Wang, C.-T. Tseng, A. S. Bhalla, and R. Guo, *J. Appl. Phys.* **103**, 084122 (2008).

¹⁶W. S. Chang, L. C. Lim, P. Yang, C.-S. Ku, H.-Y. Lee, and C.-S. Tu, *J. Appl. Phys.* **108**, 044105 (2010).

¹⁷K. K. Rajan, M. Shanthi, W. S. Chang, J. Jin, and L. C. Lim, *Sens. Actuators, A* **133**, 110 (2007).

¹⁸H. Cao, F. Bai, N. Wang, J. Li, D. Viehland, G. Xu, and G. Shirane, *Phys. Rev. B* **72**, 064104 (2005).

¹⁹H. Cao, J. Li, D. Viehland, G. Xu, and G. Shirane, *Appl. Phys. Lett.* **88**, 072915 (2006).

²⁰H. Cao, J. Li, D. Viehland, and G. Xu, *Phys. Rev. B* **73**, 184110 (2006).

²¹Z. Li, Z. Xu, X. Yao, and Z.-Y. Cheng, *J. Appl. Phys.* **104**, 024112 (2008).

²²Y. U. Wang, *Phys. Rev. B* **76**, 024108 (2007).

²³M. Shen and W. Cao, *J. Appl. Phys.* **95**, 8124 (2004).